ChemComm

COMMUNICATION

View Article Online
View Journal | View Issue

Check for updates

Cite this: *Chem. Commun.*, 2019, 55, 2688

Received 5th January 2019,
Accepted 6th February 2019

DOI: 10.1039/c9cc00113a

rsc.li/chemcomm

Published on 06 2 2019. Downloaded on 2026-05-16 1:13:57.

# A lysosome-targeting dual-functional fluorescent probe for imaging intracellular viscosity and beta-amyloid†

Hui-ya Tan,[a] Yu-tai Qiu,[a] Han Sun,[a] Jin-wu Yan*[abc] and Lei Zhang*[abc]

**A lysosome-targeting dual-functional fluorescent probe was rationally designed and developed for imaging intracellular lysosomal viscosity and beta-amyloid. More importantly, the real-time tracking of the dynamic movement of lysosomes, as vesicle structures, has been achieved using Lyso-MC.**

Alzheimer's disease (AD), an age-related condition, leads to progressive cognitive decline, a communication barrier, language disorder and loss of the ability to self-care.[1–3] Besides this, AD affects millions of people worldwide with 5 million new cases every year.[4] However, symptomatic treatment only mildly improves the symptoms of AD, but the disease itself is still incurable due to its unclear pathophysiological mechanism.[5,6] A toxic amyloid-β peptide (Aβ) is generated from the APP (amyloid precursor protein) after the sequential action of β- and γ-secretase and accumulates constantly to form senile plaques, the hallmark of AD, which are considered to be basic pathological targets for primary prevention, early diagnosis and treatment of the disease.[5,6] It has been pointed out that intracellular Aβ is involved in the early stages of AD and spreads from neuron to neuron, directly causing neurotoxicity and triggering AD.[7–9] Several studies have found that APP and Aβ are generated as a result of autophagy and the endocytic pathway.[10–13] Besides this, AD can be characterized by lysosomal dysfunction and a massive accumulation of lysosomal-related vesicles in the degenerating neurons.[11,14,15] Moreover, an increasing number of studies have pointed out that the dysfunction of the autophagy pathway is conducive to Aβ accumulation in pathological conditions.[11] Also, much evidence advocates that the lysosomal system, an acidic vesicular compartment containing various hydrolases, is related to Aβ production and neurotoxicity.[16,17] In addition, restoring autophagy or improving the lysosomal degradation of intracellular Aβ may be a potential therapeutic approach to treating AD.[10,13] Therefore, monitoring cellular lysosomal movement or physiological changes and intracellular Aβ could provide a better understanding of AD pathology and its early diagnosis.

It has been reported that lysosomal viscosity is an important benchmark for lysosome condition and reflects the status and function of this organelle.[16,18,19] Therefore, tracing the lysosome or monitoring its viscosity changes is of great benefit for AD diagnosis and pathological studies. Recently, many Aβ fluorescent probes[20–22] and many lysosome-targetable fluorescent probes used to image viscosity[19,23,24] have been reported. However, as is known, the imaging of both viscosity and Aβ aggregates at the cellular level using a lysosome-targetable dual-functional fluorescent probe has not been reported.

Herein, a fluorescent probe (**Lyso-MC**) for the sensitive imaging of intracellular lysosomes and Aβ aggregates was reasonably designed and developed. Neutral merocyanine dye (**MC-1**)[25] was selected as the fluorophore to design this probe, which was previously reported by our group as a good scaffold that has been used to image Aβ plaques *in vivo* and image viscosity at the cellular level by Lin's group.[26] However, the low quantum yield and photostability of **MC-1** restricts its further application. In this study, a 3-morpholinopropylamine moiety was rationally introduced as an electron-donor to enhance the π electron conjugation so as to improve the fluorescence quantum yield, and function as a lysosomal targeting group.[19,23,24] As is known, **Lyso-MC** was the first lysosome-targeting dual-functional probe developed to monitor viscosity and Aβ aggregates at the cellular level.

The synthesis of **Lyso-MC** is outlined in Scheme S1 (ESI†) and its structure (Scheme 1) was confirmed by $^{1}$H and $^{13}$C NMR spectroscopy and high-resolution mass spectrometry (HR-MS). The fluorescence response spectra of **Lyso-MC** were first investigated in a water–glycerol system with increasing viscosity. As shown in Fig. 1A, **Lyso-MC** exhibits its weakest fluorescence emission at

[a] *School of Biology and Biological Engineering, South China University of Technology, Guangzhou 510006, P. R. China*
[b] *Guangdong Provincial Engineering and Technology Research Center of Biopharmaceuticals, South China University of Technology, Guangzhou 510006, P. R. China*
[c] *Joint International Research Laboratory of Synthetic Biology and Medicine, South China University of Technology, Guangzhou 510006, P. R. China. E-mail: yjw@scut.edu.cn, lzhangce@scut.edu.cn*

† Electronic supplementary information (ESI) available: Synthesis and characterization of the probe, experimental procedures, and supplemental spectra and graphs. See DOI: 10.1039/c9cc00113a


This journal is © The Royal Society of Chemistry 2019

Published on 06 2 2019. Downloaded on 2026-05-16 1:13:57.

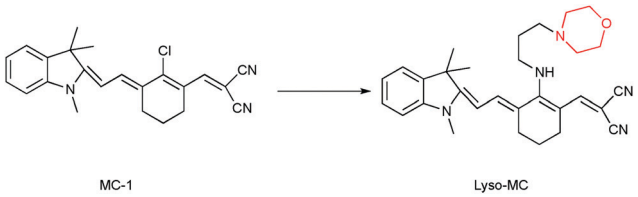


Scheme 1 Chemical structures of **MC-1** and **Lyso-MC**.

615 nm in water. Meanwhile, the emission intensity showed a dramatic fluorescence enhancement (33-fold, Table S1, ESI†) and the emission wavelength red-shifted to 620 nm due to an increase in the viscosity caused by an increase in the ratio of glycerol to water in the water–glycerol system. In addition, as shown in Fig. 1B, a good linear relationship between $\log I_{620}$ and $\log \eta$ ($R^2 = 0.99$, $x = 0.53$) was quantitatively observed according to the Förster–Hoffmann equation. Moreover, as shown in Fig. S2 (ESI†), the polarity environment only had an influence on the emission wavelength; **Lyso-MC** exhibited longer absorption and emission wavelengths upon an increase in the polarity of the surrounding environment. Compared with the strong fluorescence of **Lyso-MC** in glycerol, its fluorescence in other solvents with different polarities was negligible (Fig. S3, ESI†), therefore, its fluorescence intensity was insensitive to polarity changes. In the pH titration experiment, **Lyso-MC** was not disturbed by the lysosomal pH range (pH = 4.5–5.0) and was only affected by viscosity (Fig. S4, ESI†). Besides this, **Lyso-MC** was not affected by any interference from various amino acids and ions (Fig. S5, ESI†), exhibiting good selectivity towards viscosity. These results indicated that the **Lyso-MC** is a stable fluorescent probe for detecting viscosity in lysosomes.

We further investigated the fluorescence response of **Lyso-MC** towards the synthetic $A\beta_{1-42}$ aggregates, Aβ monomer, BSA and HSA. As expected, the probe exhibited a remarkable (10-fold) fluorescence intensity in the presence of $A\beta_{1-42}$ aggregates at a low final concentration of 0.25 μM. As displayed in Fig. S5 (ESI†), lower fluorescence responses were observed upon interaction with BSA, HSA and Aβ monomer, indicating low nonspecific binding and its good selectivity towards $A\beta_{1-42}$ aggregates. Next, the interaction between **Lyso-MC** and $A\beta_{1-42}$ aggregates was further studied by carrying out fluorescence titrations. As shown in Fig. 1C, upon titration with $A\beta_{1-42}$ aggregates, the emission wavelength blue-shifted to 610 nm and the emission intensity was significantly enhanced. Besides this, it showed a good linear relationship ($R^2 = 0.9899$) with $A\beta_{1-42}$ aggregates in the concentration range of 0 to 2.5 μM (Fig. 1D). Moreover, the detection limit of **Lyso-MC** was determined to be as low as 10.2 nM (Table S2, ESI†). After the saturation binding assay between **Lyso-MC** and $A\beta_{1-42}$ aggregates, the binding constant was calculated to be 31.74 nM, indicating that the **Lyso-MC** probe exhibited moderate affinity towards the Aβ aggregates (Table S2, ESI†). In addition, the log *P* value was measured to be 2.63, predicting that **Lyso-MC** has the potential for good blood–brain barrier (BBB) penetration. Besides this, red and blue shifts were observed for **Lyso-MC** in viscous and hydrophobic environments, respectively, therefore it could be used as a dual-functional fluorescent probe to distinguish viscosity changes and Aβ aggregates on the basis of the different emission wavelengths in the different environments.

Due to its good response to viscosity, we further investigated the application of **Lyso-MC** in living cells. Before fluorescence imaging in living cells, the cytotoxicity of **Lyso-MC** was first assessed in SH-SY5Y and HeLa cells. A standard MTT assay in SH-SY5Y and HeLa cells showed that over 80% of the cells remained alive when 12.5 μM of **Lyso-MC** was internalized for 12 h (Fig. S7, ESI†), indicating that the probe exhibited weak cytotoxicity. Then, the fluorescence imaging of **Lyso-MC** in living SH-SY5Y and HeLa cells was performed by confocal laser scanning microscopy (CLSM). The cells exhibited negligible fluorescence in the absence of **Lyso-MC**, while the cells incubated with **Lyso-MC** exhibited strong red fluorescence and the fluorescence intensity was found to be dose and time dependent, indicating that **Lyso-MC** permeated the membrane and stained the living cells (Fig. S8 and S9, ESI†).

Encouraged by the good membrane-permeability of the probe, we further investigated the co-localization of **Lyso-MC** in lysosomes of SH-SY5Y cells with commercially available LysoTracker Green DND-26 and MitoTracker Green FM. As shown in Fig. 2, **Lyso-MC** overlapped very well with LysoTracker Green, showing an overlap coefficient of as high as 0.96 between **Lyso-MC** and LysoTracker Green, while the coefficient between **Lyso-MC** and MitoTracker green was only 0.53. The results indicated that **Lyso-MC** is a lysosome-targetable probe. Meanwhile, we investigated the photostability of **Lyso-MC** inside the cells, which is of great importance for imaging the viscosity of lysosomes. Then, commercially-available LysoTracker Green was used as a comparison. The SH-SY5Y cells were exposed to the 561 nm channel after incubating with **Lyso-MC**, while the LysoTracker Green group was exposed to the 488 nm channel. After 10 min of continuous illumination, the signal losses for **Lyso-MC** and LysoTracker Green were 72% and 88%, respectively (Fig. S10, ESI†). Therefore, the probe exhibited moderate photostability both in solution (Fig. S6, ESI†) and in living cells.

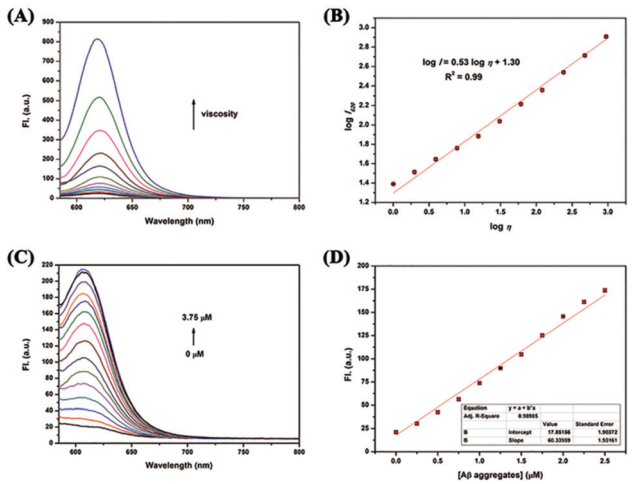


Fig. 1 (A) Solvent viscosity-dependent fluorescence changes of **Lyso-MC** (0.25 μM) in a water–glycerol system, (B) the linear relationship between $\log I_{620}$ and $\log \eta$ of **Lyso-MC**, (C) fluorescence spectroscopic titration of **Lyso-MC** (0.25 μM) towards $A\beta_{1-42}$ aggregates in PBS buffer (pH = 7.4), (D) emission intensity of **Lyso-MC** as a function of the concentration of $A\beta_{1-42}$ aggregates in PBS buffer (pH = 7.4).

Published on 06 2 2019. Downloaded on 2026-05-16 1:13:57.

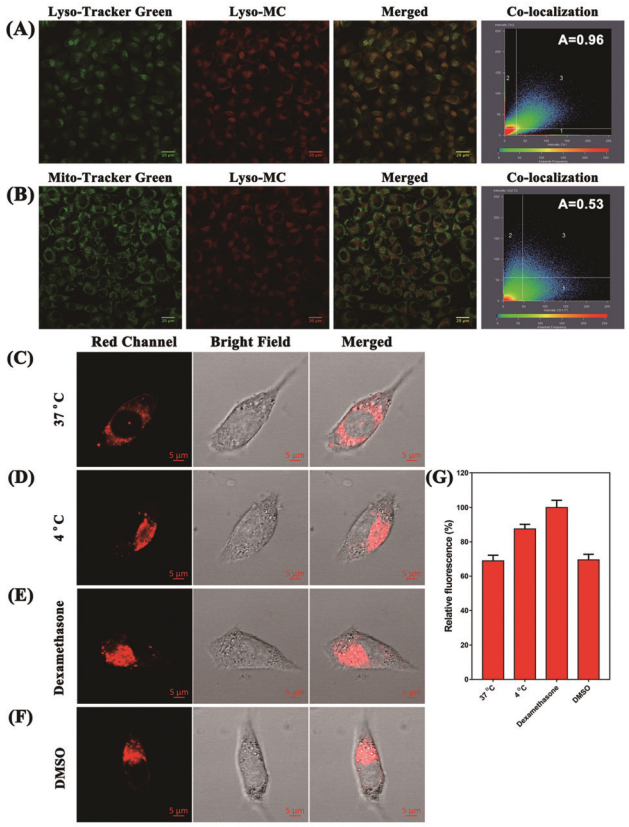


Fig. 2 (A) Colocalization fluorescence images of SH-SY5Y cells co-incubated with **Lyso-MC** (5 μM) and LysoTracker Green (1 μM), (B) colocalization fluorescence images of SH-SY5Y cells co-incubated with **Lyso-MC** (5 μM) and MitoTracker Green (1 μM). Scale bars: 20 μm, (C) confocal fluorescence images of SH-SY5Y cells incubated with **Lyso-MC** (5 μM) only at 37 °C, (D) confocal fluorescence images of SH-SY5Y cells incubated with **Lyso-MC** (5 μM) only at 4 °C, (E) cells were incubated with **Lyso-MC** (5 μM) only at 37 °C for 30 min followed by treatment with dexamethasone (5 μM) for another 10 min, (F) cells were incubated with **Lyso-MC** (5 μM) only at 37 °C for 30 min followed by treatment with DMSO (10 μL) for another 30 min, and (G) analysis of the relative fluorescence intensity in SH-SY5Y cells treated in different incubation situations ($n$ = 3, data were obtained from ImageJ Software), scale bars: 5 μm.

It is known that a lower temperature contributes to an increase in the intracellular viscosity and that dexamethasone when used as a clinic drug has been proven to be effective in increasing lysosomal viscosity.[27,28] With the aim of investigating the ability of **Lyso-MC** to monitor the variation in the intracellular lysosomal viscosity, living SH-SY5Y cells were first incubated with the probe (5 μM) at different temperatures. As shown in Fig. 2, the cells incubated at 4 °C exhibited a stronger red fluorescence in the red channel when compared with the cells at 37 °C due to the greater viscosity exhibited at 4 °C. As a result, **Lyso-MC** was only able to detect the lysosomal viscosity in living cells. Besides this, it was clearly observed that the fluorescence intensity increased after treatment with dexamethasone (5 μM), indicating that the lysosomal viscosity was greater than that at 37 °C. In addition, there were no obvious fluorescence changes when incubated with DMSO (10 μL) compared with being incubated with the probe at 37 °C, which further demonstrated that the probe could be used to monitor the variation in the lysosomal viscosity without any interference from polarity fluctuation in living cells.

Due to the good lysosome-targeting performance of the probe, we investigated the ability of the probe to trace lysosomes in real time and observed the subcellular structure of the lysosomes using CLSM in ultra-high-resolution mode. Images of the SH-SY5Y cells incubated with **Lyso-MC** were taken every 4 seconds by CLSM. As shown in Fig. 3, it can be seen that the dynamic lysosomes in living cells have vesicular structures and five different colors were used to clearly show the movements of the lysosomes at various time points (0, 20, 40, 60 and 80 s). The merged images at various time points and dynamic video indicate that the movements of the lysosomes were rather active and that **Lyso-MC** could be used to trace intracellular lysosomes in real-time.

Considering the specific binding of the probe to $A\beta_{1-42}$ aggregates in solution and the important pathological action of intracellular Aβ aggregates, PC12 cells transfected for the overexpression of Aβ (PC12-EGFP-Aβ cells) and normal PC12 cells taken as controls were used to investigate whether **Lyso-MC** could detect Aβ aggregates at the cellular level. As shown in Fig. S11B (ESI†), granular aggregates were detected with **Lyso-MC** in the cytoplasm, consistent with an immunofluorescence group (Fig. S11A, ESI†). Meanwhile, there was negligible fluorescence observed in the control PC12 cells (Fig. S12, ESI†). Besides this, there was also no fluorescence observed in the PC12-EGFP-Aβ cells with no staining with **Lyso-MC** or immunofluorescence (Fig. S13, ESI†). We also conducted a co-localization experiment for Aβ aggregates in the transfected PC12-EGFP-Aβ cells through co-staining with **Lyso-MC** after immunofluorescence assay with the secondary antibody Alexa Fluor®405. As shown in Fig. 4, the **Lyso-MC** and Alexa Fluor®405 merged well with a good Pearson's coefficient of 0.7997. The ICA (intensity correlation analysis, which was used to evaluate the intensity distribution of the two co-existing stains) plots for the **Lyso-MC** and Alexa Fluor®405 created an unsymmetrical hourglass-shaped scatterplot, which tended toward positive values (Fig. 4G and H). No matter whether *ex situ* monitored or co-localized for Aβ aggregates, the **Lyso-MC** probe was confirmed to detect Aβ aggregates at the cellular level.

In conclusion, a red-emitting dual-functional fluorescent probe with low cytotoxicity based on a neutral merocyanine dye (**MC-1**) was rationally designed and developed for imaging intracellular lysosomal viscosity and Aβ aggregates. The spectral results showed that **Lyso-MC** exhibited an excellent linear relationship between the logarithm of fluorescence intensity and the logarithm of viscosity ($R^2$ = 0.99, $x$ = 0.53). Meanwhile, the probe also showed a significant turn-on fluorescence response when bound to Aβ aggregates and a high sensitivity towards Aβ aggregates (detection limit: 10.2 nM). Besides this, **Lyso-MC** was applied to monitor lysosomal viscosity changes and detect intracellular Aβ aggregates. More importantly, the real-time tracking of the dynamic movement of lysosomes, as vesicle structures, was achieved using **Lyso-MC**. Taking advantage of its remarkable properties, this versatile probe could be a promising imaging tool for use in Alzheimer's disease pathology-related fields.

This work was financially supported by the Natural Science Foundation of Guangdong Province, China (2016A030310463 and 2016A010121004), the National Natural Science Foundation of China (21502056) and the Medical Scientific Research Foundation of Guangdong Province, China (A2018080).

 This journal is © The Royal Society of Chemistry 2019

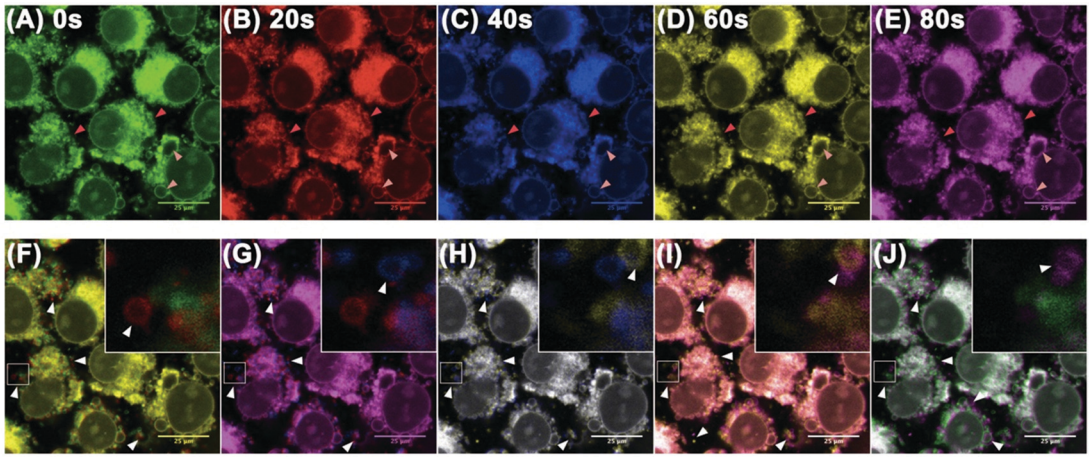


Fig. 3 (A–E) Confocal images of SH-SY5Y cells stained with 5 μM **Lyso-MC** for 30 min. Different colors were used to illustrate the fluorescence images at 20, 40, 60 and 80 s, respectively. (F–J) Merging of the images at two different time points: (F) 0 and 20 s, (G) 20 and 40 s, (H) 40 and 60 s, (I) 60 and 80 s, and (J) 0 and 80 s. The inset shows the zoomed-in image. The dark pink and light pink arrow heads indicate the different sizes of the lysosomes. The white arrow heads indicate the significant movements of the lysosomes. Scale bars: 25 μm.

Published on 06 2 2019. Downloaded on 2026-05-16 1:13:57.

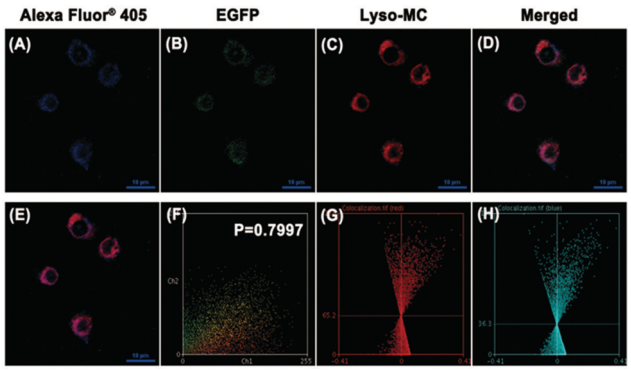


Fig. 4 Co-localization images in transfected PC12 cells after immunofluorescence for the $A\beta_{1-42}$ aggregates and then co-stained with **Lyso-MC** (1 μM). (A) Immunofluorescence image from Alexa Fluor®405, (B) fluorescence image of EGFP, (C) fluorescence image of **Lyso-MC**, (D) the merged image of (A–C), (E) the merged image of (A and C), (F) the intensity correlation plot of co-stained **Lyso-MC** and immunofluorescence, ICA plots of (G) staining by **Lyso-MC** and (H) Alexa Fluor®405 of the immunofluorescence (analyzed by ImageJ software).

## Conflicts of interest

There are no conflicts to declare.

## Notes and references

1 X. Zhang, Y. Tian, C. Zhang, X. Tian, A. W. Ross, R. D. Moir, H. Sun, R. E. Tanzi, A. Moore and C. Ran, *Proc. Natl. Acad. Sci. U. S. A.*, 2015, **112**, 9734–9739.
2 C. Ballard, S. Gauthier, A. Corbett, C. Brayne, D. Aarsland and E. Jones, *Lancet*, 2011, **377**, 1019–1031.
3 M. Staderini, M. A. Martin, M. L. Bolognesi and J. C. Menendez, *Chem. Soc. Rev.*, 2015, **44**, 1807–1819.
4 H. Tong, K. Lou and W. Wang, *Acta Pharm. Sin. B*, 2015, **5**, 25–33.
5 F. Mangialasche, A. Solomon, B. Winblad, P. Mecocci and M. Kivipelto, *Lancet Neurol.*, 2010, **9**, 702–716.
6 S. Gauthier, L. Wu, P. Rosa-Neto and J. Jia, *Transl. Neurodegener.*, 2012, **1**, 1–13.
7 J. Naslund, V. Haroutunian, R. Mohs, K. L. Davis, P. Davies, P. Greengard and J. D. Buxbaum, *J. Am. Med. Assoc.*, 2000, **283**, 1571–1577.
8 M. Koistinaho, M. Ort, J. M. Cimadevilla, R. Vondrous, B. Cordell, J. Koistinaho, J. Bures and L. S. Higgins, *Proc. Natl. Acad. Sci. U. S. A.*, 2001, **98**, 14675–14680.
9 S. Nath, L. Agholme, F. R. Kurudenkandy, B. Granseth, J. Marcusson and M. Hallbeck, *J. Neurosci.*, 2012, **32**, 8767–8777.
10 R. A. Nixon and A. M. Cataldo, *J. Alzheimer's Dis.*, 2006, **9**, 277–289.
11 R. A. Nixon, *J. Cell Sci.*, 2007, **120**, 4081–4091.
12 R. A. Nixon, D.-S. Yang and J.-H. Lee, *Autophagy*, 2008, **4**, 590–599.
13 F. Pickford, E. Masliah, M. Britschgi, K. Lucin, R. Narasimhan, P. A. Jaeger, S. Small, B. Spencer, E. Rockenstein, B. Levine and T. Wyss-Coray, *J. Clin. Invest.*, 2008, **118**, 2190–2199.
14 K. Inoue, J. Rispoli, H. Kaphzan, E. Klann, E. I. Chen, J. Kim, M. Komatsu and A. Abeliovich, *Mol. Neurodegener.*, 2012, **7**, 48.
15 J.-H. Lee, W. H. Yu, A. Kumar, S. Lee, P. S. Mohan, C. M. Peterhoff, D. M. Wolfe, M. Martinez-Vicente, A. C. Massey, G. Sovak, Y. Uchiyama, D. Westaway, A. M. Cuervo and R. A. Nixon, *Cell*, 2010, **141**, 1146–1158.
16 R. A. Nixon, A. M. Cataldo and P. M. Mathews, *Neurochem. Res.*, 2000, **25**, 1161–1172.
17 J. Han and K. Burgess, *Chem. Rev.*, 2010, **110**, 2709–2728.
18 T. Liu, X. Liu, D. R. Spring, X. Qian, J. Cui and Z. Xu, *Sci. Rep.*, 2014, **4**, 5418.
19 L.-L. Li, K. Li, M.-Y. Li, L. Shi, Y.-H. Liu, H. Zhang, S.-L. Pan, N. Wang, Q. Zhou and X.-Q. Yu, *Anal. Chem.*, 2018, **90**, 5873–5878.
20 J.-y. Zhu, L.-f. Zhou, Y.-k. Li, S.-b. Chen, J.-w. Yan and L. Zhang, *Anal. Chim. Acta*, 2017, **961**, 112–118.
21 K. Rajasekhar, N. Narayanaswamy, N. A. Murugan, K. Viccaro, H.-G. Lee, K. Shah and T. Govindaraju, *Biosens. Bioelectron.*, 2017, **98**, 54–61.
22 Y. Li, K. Wang, K. Zhou, W. Guo, B. Dai, Y. Liang, J. Dai and M. Cui, *Chem. Commun.*, 2018, **54**, 8717–8720.
23 B. Guo, J. Jing, L. Nie, F. Xin, C. Gao, W. Yang and X. Zhang, *J. Mater. Chem. B*, 2018, **6**, 580–585.
24 L. Hou, P. Ning, Y. Feng, Y. Ding, L. Bai, L. Li, H. Yu and X. Meng, *Anal. Chem.*, 2018, **90**, 7122–7126.
25 J.-w. Yan, J.-y. Zhu, K.-x. Zhou, J.-s. Wang, H.-y. Tan, Z.-y. Xu, S.-b. Chen, Y.-t. Lu, M.-c. Cui and L. Zhang, *Chem. Commun.*, 2017, **53**, 9910–9913.
26 R. Guo, J. Yin, Y. Ma, G. Li, Q. Wang and W. Lin, *Sens. Actuators, B*, 2018, **271**, 321–328.
27 S. Humphries, *Proc. Natl. Acad. Sci. U. S. A.*, 2013, **110**, 14693–14698.
28 L. Wang, Y. Xiao, W. Tian and L. Deng, *J. Am. Chem. Soc.*, 2013, **135**, 2903–2906.